A&A 579, A82 (2015)
DOI: 10.1051/0004-6361/201525885

Astronomy & Astrophysics

Chemistry in protoplanetary disks: the gas-phase CO/H_2 ratio and the carbon reservoir

L. Reboussin[1,2], V. Wakelam[1,2], S. Guilloteau[1,2], F. Hersant[1,2], and A. Dutrey[1,2]

[1] Université Bordeaux, LAB, UMR 5804, 33270 Floirac, France
e-mail: laura.reboussin@obs.u-bordeaux1.fr
[2] CNRS, LAB, UMR 5804, 33270 Floirac France

Received 13 February 2015 / Accepted 5 May 2015

ABSTRACT

Context. The gas mass of protoplanetary disks and the gas-to-dust ratio are two key elements driving the evolution of these disks and the formation of planetary system.
Aims. We explore to what extent CO (or its isotopologues) can be used as a tracer of gas mass.
Methods. We use a detailed gas-grain chemical model and study the evolution of the disk composition, starting from a dense prestellar core composition. We explore a range of disk temperature profiles, cosmic-ray ionization rates, and disk ages for a disk model representative of T Tauri stars.
Results. At the high densities that prevail in disks, we find that because of fast reactions on grain surfaces, CO can be converted to less volatile forms (principally s-CO_2, and to a lesser extent s-CH_4) instead of being evaporated over a wide range of temperature. The canonical gas-phase abundance of 10^{-4} is only reached above about 30–35 K. The dominant carbon bearing entity depends on the temperature structure and age of the disk. The chemical evolution of CO is also sensitive to the cosmic-ray ionization rate. Larger gas phase CO abundances are found in younger disks. Initial conditions, such as parent cloud age and density, have a limited impact.
Conclusions. This study reveals that CO gas-phase abundance is heavily dependent on grain surface processes, which remain very incompletely understood so far. The strong dependence on dust temperature profile makes CO a poor tracer of the gas-phase content of disks.

Key words. astrochemistry – protoplanetary disks – molecular processes

1. Introduction

Measuring the mass of protoplanetary disks remains a challenging task. Because H_2 is either unobservable in the physical conditions prevailing throughout most disks, or when detected, only sampling peculiar conditions (Bary et al. 2008), we have to rely on indirect tracers to estimate disk masses.

A common practice is based on the dust emission at mm wavelengths, where the dust opacity is moderate and thus the emission sensitive to most of the dust mass. However, the dust emissivity is not well known: it depends on dust characteristics, in particular the grain size distribution, and differential grain growth has been observed in disks (Guilloteau et al. 2011; Pérez et al. 2012), invalidating the use of a unique emissivity coefficient throughout the disk. Despite this limitation, under the simple assumption of an average emissivity of order 2 $cm^2\ g^{-1}$, it has been shown that the dust masses of protoplanetary disks scale with their host stellar mass (Andrews et al. 2013).

In any case, dust alone cannot inform us about the gas content. It is often assumed that the gas-to-dust ratio is of order 100 to derive disk masses, but many processes (such as the vertical dust settling and the radial drift of large grains) may affect the gas-to-dust ratio. HD is perhaps the best proxy for H_2, and has been detected so far in TW Hya (Bergin et al. 2013). However, the interpretation is strongly dependent on the thermal profile of the disk. Furthermore, there is no longer any telescope that is sensitive enough to detect it in more distant protoplanetary disks.

Early studies of disk emission found that the ^{13}CO lines were much fainter than expected from mm continuum emission from dust (Beckwith et al. 1990; Dutrey et al. 1996). Part of this discrepancy may be attributable to different disk sizes in dust and continuum (Piétu et al. 2006, 2007; Hughes et al. 2009), but depletion of CO on dust grains was invoked as the main cause.

Recently, Williams & Best (2014) suggested that, because of its relatively simple chemistry, CO could be a reliable tracer of dust mass. They argued that gas-phase CO abundance depends mostly on gas temperature, and that with a reasonable knowledge of the disk thermal structure, the fraction of carbon locked up in gas-phase CO can be evaluated (10^{-4} where $T > 20$ K). Apart from the upper layers, which contain little mass, the thermal structure in disks is dominated by dust (Chiang & Goldreich 1997) and can be reasonably well constrained from SED measurements. Exploring a large grid of disk parameters, Williams & Best (2014) concluded that disk gas masses were in general rather small, leading to an average gas-to-dust ratio well below the canonical value of 100 found in the interstellar medium.

However, this finding contradicts the high mass suggested by the analysis of the HD observations of TW Hya (Bergin et al. 2013). To resolve the discrepancy between these two approaches, a very low CO to H_2 ratio is required. Very low apparent CO to dust ratios were also found by Chapillon et al. (2008) for CQ Tau and MWC 758, two Herbig Ae stars, as well as for BP Tau (Dutrey et al. 2003), despite large temperatures (above 30 K) deduced from CO. Under the simple assumption

that CO is mostly in the gas phase because of high temperatures, Chapillon et al. (2010) showed that the lack of detection of CI in CQ Tau excludes photodissociation as the sole cause of low CO column densities, and implies a very low gas-to-dust ratio.

Since CO rotational transitions are generally very optically thick in disks, using the less abundant isotopologues is required to sample the gas content. This introduces a significant complexity because of the different shielding of the isotopologues against photodissociation by the UV radiation field. Another added complexity is the ^{13}CO fractionation that can occur in lukewarm regions (20–30 K). These processes have been studied in detail in Miotello et al. (2014), who showed that these effects have a substantial impact on the derivation of the CO gas content and could reduce the discrepancy between the two approaches.

Favre et al. (2013) concluded that the emission of C^{18}O in TW Hya could only be explained assuming CO has been converted to other hydrocarbons, rather than released from grains. As an other alternative, Chapillon et al. (2008) suggested that because large grains can remain cold, CO might remain trapped in these grains even in relatively warm disks, like those around the Herbig Ae stars CQ Tau or MWC 758.

Given that other molecules suffer from an even more complex chemistry than CO and its isotopologues, it is important to understand to what extent CO can be a tracer of disk masses.

In this paper, we re-explore this issue using a detailed gas-grain chemical network. We concentrate here on some aspects of chemistry that can affect the (gas-phase) CO abundance in protoplanetary disks. We first study the impact of temperature profile and the role of grain surface chemistry for disks of different ages. Second, we evaluate the importance of initial conditions on the time-dependent disk chemistry.

Our purpose is not to build complete disk models, but to reveal the importance of these effects on the chemical evolution of protoplanetary disks. The paper is organized as follows. In Sect. 2, we describe our chemical model and the physical disk structure used for this work. In Sect. 3, we present the effect of the disk vertical temperature profile on the chemistry of carbon-bearing species, as well as the impact of the cosmic-ray ionization rate and the age of the disk. We also study the sensitivity of our model to the initial C/O ratio, the gas density, and the age of the parent molecular cloud. Section 4 contains a discussion of our work. Finally, in Sect. 5 we present our conclusions about this work.

2. Modeling

2.1. Chemistry

2.1.1. Model description

We used the Nautilus chemical model (Semenov et al. 2010; Reboussin et al. 2014), which computes the abundance of species as a function of time in the gas phase and at the surface of the grains. The model includes pure gas-phase chemistry with bimolecular reactions, ionizations, and dissociations by direct impact of cosmic ray particle and UV photons (interstellar FUV photons and secondary UV photons induced by cosmic ray/H_2 interactions). We assume the standard cosmic-ray ionization rate $\zeta_{CR} = 1.3\times10^{-17}$ s^{-1}. The dust grains are represented by spherical particles with a radius of 0.1 μm, a density of 3 g cm^{-3}, and are made of amorphous olivine. The gas and dust temperatures are assumed to be the same and we use a gas-to-dust mass ratio of 100. The gas-grain interactions include adsorption of gas-phase species, those species can desorb back into the gas-phase by thermal desorption and nonthermal desorption (via the energy released by exothermic surface reactions and cosmic ray induced desorption). The impact of photodesorption is discussed in Sect. 3.2. The model takes grain-surface reactions with diffusion reactions at the surface of the dust particle via thermal hopping into account (we do not take diffusion by quantum tunneling into account). The energy barrier between two adjacent sites is taken as half of the binding energy (Garrod & Herbst 2006). Photodissociation on the surface by UV photons and cosmic ray induced UV field are also considered.

Table 1. Initial abundances used in our model.

Element	Abundance relative to H	
H_2	0.5	
He	9×10^{-2} [a]	
N	6.2×10^{-5} [b]	
O	3.3×10^{-4} [c]	(C/O = 0.5)
	1.4×10^{-4} [c]	(C/O = 1.2)
C^+	1.7×10^{-4} [b]	
S^+	8×10^{-9} [d]	
Si^+	8×10^{-9} [d]	
Fe^+	3×10^{-9} [d]	
Na^+	2×10^{-9} [d]	
Mg^+	7×10^{-9} [d]	
P^+	2×10^{-10} [d]	
Cl^+	1×10^{-9} [d]	

Notes. [(a)] See discussion in Wakelam & Herbst (2008). [(b)] Jenkins (2009). [(c)] See discussion in Hincelin et al. (2011). [(d)] Low metal abundances (Graedel et al. 1982).

2.1.2. Cloud model parameters

To obtain the initial chemical composition of the disk, we first compute the chemical composition of the parent molecular cloud. We run Nautilus during 10^6 yr for typical dense cloud conditions as our nominal cloud: a gas density of $n_H = n(H) + 2n(H_2) = 2\times10^4$ cm^{-3}, a temperature of 10 K (with $T_{gas} = T_{dust}$), a visual extinction of 10, a cosmic-ray ionization rate of 1.3×10^{-17} s^{-1}, and the initial abundances as listed in Table 1. For all elements but He, N, C, and O, we used the "low metal" elemental abundances defined by Graedel et al. (1982). For oxygen, two values have been considered: a "low depletion" case, which corresponds to C/O = 0.5 in our standard model, and a "high depletion" case, which corresponds to C/O = 1.2 considered in Sect. 3.5.2. The helium abundance is assumed to be 0.09 (Wakelam & Herbst 2008), while the nitrogen and carbon abundances are extrapolated from Jenkins (2009) up to a density of 2×10^4 cm^{-3} (see discussion in Hincelin et al. 2011).

2.1.3. Chemical network

The chemical network used for this work contains 8624 reactions: 6844 are pure gas-phase reactions and 1780 are grain-surface and gas-grain interactions. The model follows the chemistry of 703 species (atoms, radicals, ions and molecules): 504 are gas-phase species and 199 are species on grains. The surface network is based on Garrod et al. (2007) whereas the gas-phase network is based on kida.uva.2011 with updates from Wakelam et al. (2013) and Loison et al. (2014a,b). We have added 19 gas-phase species and 377 pure gas-phase reactions (mainly carbon and nitrogen chains). The network is available on the KInetic Database for Astrochemistry (KIDA) website[1].

[1] http://kida.obs.u-bordeaux1.fr/models

2.2. Disk structure

For the disk physical parameters, we used the disk model described in Hersant et al. (2009). The vertical density structure is obtained by integrating the equation of hydrostatic equilibrium,

$$\frac{\partial \ln \rho}{\partial z} = -\left[\left(\frac{GM_* z}{r^3}\right)\left(\frac{\mu m_{\rm H}}{k_{\rm B} T}\right) + \frac{\partial \ln T}{\partial z}\right], \quad (1)$$

where G is the gravitationnal constant, $M_* = 0.5\ M_\odot$ is the mass of the central star, $\mu = 2.4$ is the reduced mass of total hydrogen, $m_{\rm H}$ the mass of the proton, and $k_{\rm B}$ the Boltzmann constant.

For the isothermal case, the vertical density is given by

$$\rho(z) = \rho_0 \exp -\left(\frac{1}{2}\left(\frac{z}{H}\right)^2\right), \quad (2)$$

where $H = (k_B T_{\rm mid} r^3 / G M_* \mu m_{\rm H})^{1/2}$ is the pressure scale height derived from the midplane temperature $T_{\rm mid}$.

We assumed the disk surface density to vary as $r^{-1.5}$ described in Hersant et al. (2009) as follows:

$$\Sigma(r) = \Sigma_{100}\left(\frac{r}{100\ {\rm au}}\right)^{-1.5} \ {\rm g\ cm^{-2}}, \quad (3)$$

with $\Sigma_{100} = 0.8\ {\rm g\ cm^{-2}}$. The hydrogen surface density is given by $\Sigma_{100} = \mu m_{\rm H} N_{100}(H)$ in which μ is the mean weight per H nuclei, which we approximate as $\mu/2$. Thus, $N_{100}(H) \approx 4 \times 10^{23}\ {\rm cm^{-2}}$. With an outer radius of 700 au, the disk mass is $M_{\rm d} = 0.03\ M_\odot$.

Contrary to Hersant et al. (2009), we use the disk temperature structure as described in Williams & Best (2014). The radial midplane temperature $T_{\rm mid}$ and the atmospheric temperature $T_{\rm atm}$ (temperature at $z \geq 4H$) are given as a power law of the radius:

$$T_{\rm mid}(r) = T_{\rm mid,1}\left(\frac{r}{1\ {\rm au}}\right)^{-q}, \quad (4)$$

$$T_{\rm atm}(r) = T_{\rm atm,1}\left(\frac{r}{1\ {\rm au}}\right)^{-q}, \quad (5)$$

with $q = 0.55$, which leads to a flaring exponent of 1.23.

A sine function is used for the connection between the midplane and the atmosphere gas temperatures:

$$T(r,z) = \begin{cases} T_{\rm mid} + (T_{\rm atm} - T_{\rm mid})\left[\sin\left(\frac{\pi z}{2 z_q}\right)\right]^{2\delta} & \text{if } z < z_q \\ T_{\rm atm} & \text{if } z \geq z_q, \end{cases} \quad (6)$$

with $\delta = 2$ (steepness of the profile) and $z_q = 4H$ (height at which the disk reaches the atmospheric value). The visual extinction is related to the total column density of hydrogen by $A_V = N(H)/1.6 \times 10^{21}\ {\rm cm^{-2}}$, following Wagenblast & Hartquist (1989), consistent with the adopted mean grain radius of 0.1 μm. Changing the temperature profile also affects the density and visual extinction distributions.

For the UV radiative transfer in the disk, we consider only the vertical extinction. We assume that the radial extinction of stellar UV field is very efficient so that UV photons are scattered by small grains at high altitudes. The UV flux is decreasing as $1/r^2$ from the central star. We consider $G_0 = 410$ for the field for a distance of 100 au from the star: this is representative of low mass T Tauri stars like DM Tau. Half of this flux is assumed to be scattered downward inside the disk. To model the CO and H_2 UV self-shielding, we used the approximation from Lee et al. (1996). We use 64 points in the vertical direction.

Table 2. Model descriptions.

Model 1	$T_{\rm gas} = T_{\rm dust}$ Weak temperature gradient defined as: $T_{\rm atm,1} = T_{\rm mid,1} + 300\ {\rm K}^a$
Model 2	$T_{\rm gas} = T_{\rm dust}$ Strong temperature gradient defined as: $T_{\rm atm,1} = T_{\rm mid,1} + 1000\ {\rm K}^a$
Model 3	$T_{\rm gas} > T_{\rm dust}$ Dust temperature profile as in Model 1. Gas temperature profile as in Model 2.

Notes. [(a)] For $r = 1$ au.

Table 3. Molecular binding (desorption) energies.

Species	E_D (K)
C	800
CO	1150
CH_4	1300
H_2CO	2050
CO_2	2575
CH_3CCH	3837
C_2H_6	4387
CH_3OH	5534

We created a large grid of models by varying the values of $T_{\rm mid,1}$ and $T_{\rm atm,1}$. The disk midplane temperature is therefore ranging between 4 and 52 K while the temperature in the upper layer is ranging between 17 and 95 K (at 300 au). We also considered different models (see Table 2 for a description of our models). Model 1 is considered our nominal model. In Model 2, we study the impact of the steepness of the temperature profile taken as stronger in this model by increasing the value of $T_{\rm atm,1}$. A third model (Model 3) was considered in which the dust temperature has been considered as different from the gas temperature. In that case, the gas temperature is assumed to follow the strong gradient temperature of Model 2, while the dust temperature follows that of Model 1. Figure 1 shows the disk temperature, visual extinction, and density vertical profiles at 300 au for some of those models. Depending on the temperature profile considered, disks have different height, and the warmer disks are thicker. From coldest to the warmest, shown in Fig. 1, the disk heights at 300 au are respectively, 29, 62, and 88 au.

3. Results

In this section, we present the results obtained with our models. First, we study the impact of the temperature profile on the disk chemistry and, more particularly, on the carbon-bearing species abundances. Second, we show the sensitivity to the initial cloud composition. The initial chemical conditions used for disk modeling are listed in Table 4. Hereafter, for any molecule X, we shall use s-X to refer to molecules trapped on grains, and X for molecule in the gas-phase.

3.1. Impact of the vertical temperature profile

The (gas-phase) CO vertical abundance at $r = 300$ au is represented in Fig. 2 for the six profiles shown in Fig. 1 and for a disk age of 1 Myr. In the upper layer of the disk, the CO abundance

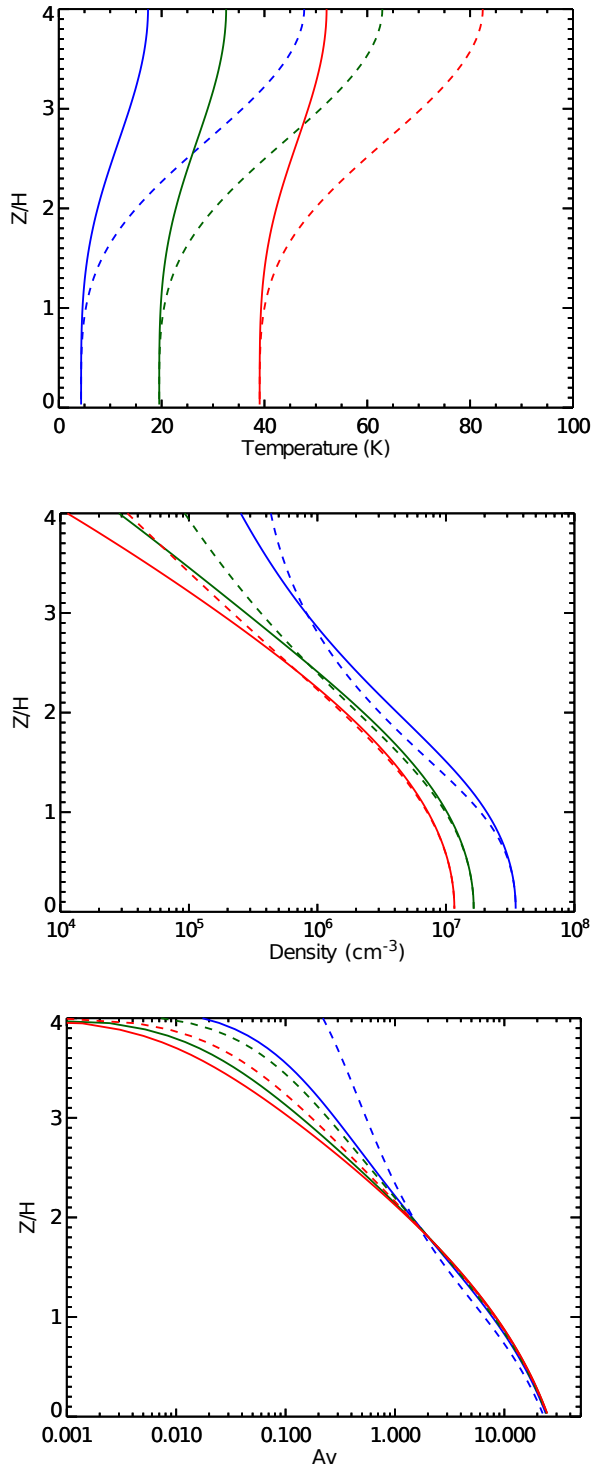

Fig. 1. Examples of temperature, density, and visual extinction vertical profiles in the protoplanetary disk at 300 au used for the chemical modeling. Solid lines are for Model 1 and dashed lines for Model 2 (see Table 2). The vertical profiles for these two models are shown for three different values of the midplane temperature $T_{\rm mid}$ at 300 au: ~4 K (blue lines), ~20 K (green lines), and ~40 K (red lines). Disk heights depend on the temperature: from the coldest to the warmest model, the disk heights are 29, 62 and 88 au at 300 au.

is mostly affected by the photodissociation process. Because of different scale heights, the visual extinction at Z/H = 4 varies between models (see Fig. 1). In the upper layer, CO is more efficiently photodissociated by UV photons for the warmer models (green and red) because the visual extinction is smaller.

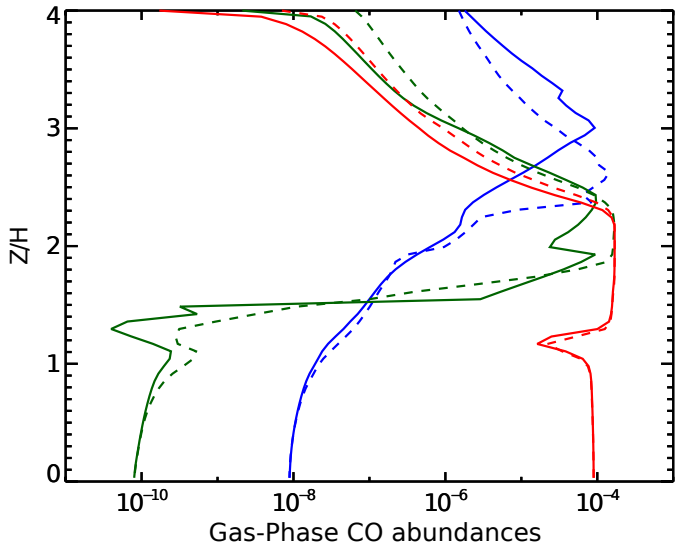

Fig. 2. Vertical gas-phase CO abundances (relative to total hydrogen) at 300 au for a disk age of 1 Myr. The color coding corresponds to the vertical profiles shown in Fig. 1. Solid lines are for Model 1 and dashed lines for Model 2 (see Table 2).

The largest CO abundances are obtained in the warm molecular layer, whose height and thickness differs according to the model. The coldest model with a stronger temperature gradient (blue dashed line in Fig. 2) shows a larger CO abundance at smaller scale height compared to the coldest model with a weak temperature gradient (blue solid line in Fig. 2). This is because the desorption temperature of CO is reached at a smaller height. In the disk midplane, the larger CO abundance is obtained with the higher $T_{\rm mid}$ model (in red in Fig. 1) because of a more efficient desorption of s-CO from the ices. For this model, the CO depletion is small, as expected at these high temperatures. The CO abundance obtained with the smaller $T_{\rm mid}$ model (in blue in Fig. 1) is higher than the intermediate model (green). In fact, at approximately 15 K, s-CO is destroyed on the dust grains to form more complex species by secondary UV photons induced by cosmic rays, such as s-CO_2, s-H_2CO and s-CH_3OH, whereas when the temperature is too low (below 9 K), the diffusion of the species, even atomic hydrogen, is less efficient at the surface of the grains.

The CO abundance profiles obtained with the models are then sensitive to the vertical temperature profile that is assumed: the midplane temperature as well as the steepness of the gradient. For midplane temperatures larger than 20 K, the steepness of the gradient no longer substantially affects the CO abundance because the evaporation temperature of s-CO is reached in the molecular layer.

For the models displayed in Fig. 2, only the warmest (red lines) reach the value $CO/H_2 = 10^{-4}$. For the other models, which are colder, this ratio is much smaller for two main reasons. Firstly, the warm molecular layer in which larger CO abundances are obtained is less extensive than in the case of warmer models, and, secondly, the CO depletion due to freeze-out and grain surface chemistry is very efficient in the disk midplane.

Figure 3 represents the disk column densities and vertical abundances (computed from the molecular column densities and the total H column density) of some carbon-bearing species in the gas phase and at the surface of the grains as a function of the disk midplane temperature and for the three models as described in Table 2. The results are obtained for a disk age of 1 Myr.

Table 4. Predicted abundances in the molecular cloud considering different model parameters.

	Abundances[a] (with respect to n_H)				
Species	Nominal cloud	C/O = 1.2	10^5 yr	10^7 yr	$n_H = 2 \times 10^5$ cm^{-3}
CO	2.4(–5)	1.3(–5)	7.2(–5)	2.9(–7)	2.2(–6)
CH_4	1.5(–7)	4.0(–7)	4.5(–7)	6.5(–7)	2.4(–8)
CO_2	3.3(–8)	6.0(–9)	4.7(–8)	9.2(–11)	7.9(–10)
C	3.1(–8)	7.0(–8)	2.9(–5)	5.4(–8)	1.4(–8)
C^+	4.2(–9)	8.0(–10)	2.0(–9)	1.2(–13)	4.4(–10)
C_2H_6	6.2(–9)	7.1(–9)	7.1(–11)	1.2(–8)	8.3(–9)
H_2CO	9.8(–9)	1.8(–8)	4.5(–8)	1.6(–9)	2.3(–9)
CH_3OH	7.1(–10)	1.0(–9)	7.2(–11)	6.2(–11)	1.1(–10)
s-CO	7.2(–5)	3.0(–5)	2.5(–5)	1.9(–7)	9.9(–5)
s-CH_4	8.5(–6)	2.5(–5)	4.2(–6)	9.2(–5)	5.1(–6)
s-CO_2	1.6(–6)	5.6(–8)	8.1(–7)	3.9(–9)	2.3(–6)
s-C_2H_6	3.4(–6)	3.9(–6)	3.9(–8)	6.4(–6)	4.6(–6)
s-H_2CO	2.8(–5)	4.1(–5)	1.8(–6)	1.0(–6)	2.3(–5)
s-CH_3OH	9.7(–6)	1.6(–5)	5.0(–7)	2.5(–6)	5.8(–6)
s-CH_3CCH	2.4(–6)	6.1(–6)	1.0(–6)	4.6(–6)	1.0(–6)

Notes. [(a)] $a(b)$ represents $a \times 10^b$.

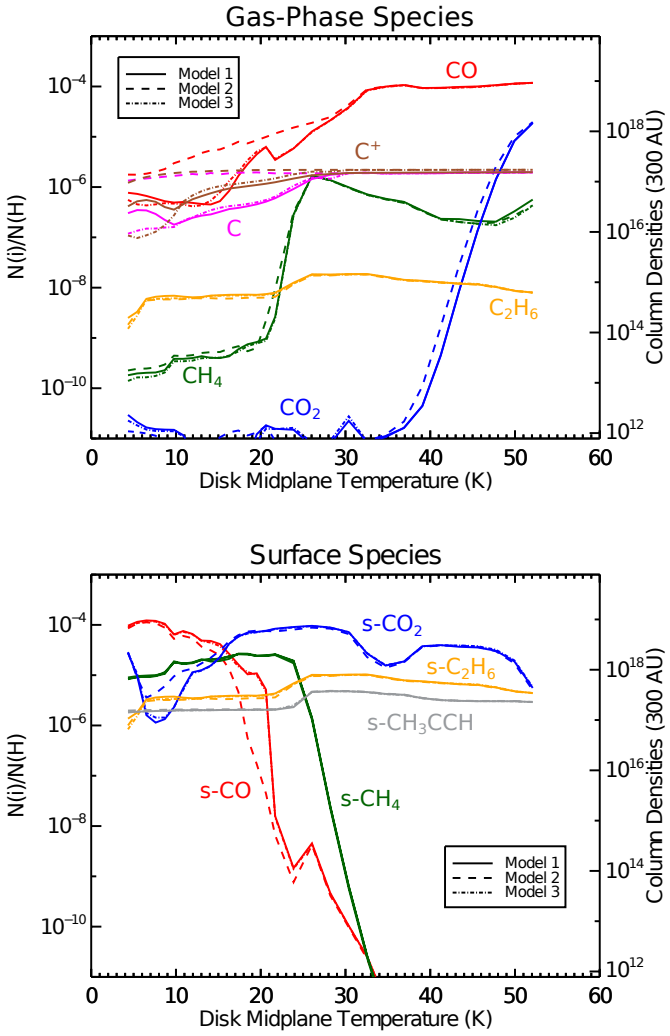

Fig. 3. Average abundances and integrated column densities (cm^{-2}) of carbon-bearing species in the gas-phase and on the grain surfaces for Model 1, 2, and 3 as a function of the disk midplane temperature (T_{mid}). s- refers for surface species. Those results are obtained at 300 au for our nominal cloud and for a disk age of 1 Myr.

In the case of temperature profiles with a midplane temperature between 5 and ~15 K in Model 1, s-CO is the most abundant C-bearing species. At higher temperatures, its abundance decreases because it is converted into other C-bearing molecules such as s-CH_4. The direct photodissociation of CO in the gas and at the surface of the grains increases the abundance of neutral carbon, and subsequent hydrogenation of carbon on the surfaces contributes to form s-CH_4. Above 15 K, s-CO_2 becomes the most abundant molecule. Its formation is due to the following reactions, for which the efficiencies are increased by 10 to ~20 orders of magnitude at such temperatures compared to 15 K:

$$\text{s-O} + \text{s-CO} \rightarrow \text{s-CO}_2, \quad (7)$$

$$\text{s-O} + \text{s-HCO} \rightarrow \text{s-CO}_2 + \text{s-H}, \quad (8)$$

$$\text{s-OH} + \text{s-CO} \rightarrow \text{s-CO}_2 + \text{s-H}. \quad (9)$$

Reaction 7 is the main formation path of s-CO_2 in our model although it must overcome a large activation energy barrier (1000 K). Reaction 8, being without a barrier, also contributes to form s-CO_2 efficiently. Reaction 9 must overcome a small activation energy barrier (80 K). The warm dust temperature enables the increase of the mobility of species at the surface of the grains and the diffusion becomes much more efficient. However, the dust temperature is not warm enough to desorb the s-CO_2 back into the gas phase. At even higher temperatures (above 30 K), CO in gas-phase is the reservoir of C because of efficient desorption and the lack of sticking on the grains.

Model 3 (in which $T_{gas} > T_{dust}$) produces species abundances very similar to Model 1 whatever T_{mid}, meaning that it is the grain temperature that is the important parameter here. For temperatures between 25 and 50 K (depending on the molecule), the steepness of the temperature gradient does not influence the computed abundances in the gas phase nor at the surface of the grains. For T_{mid} smaller than 25 K, the gas-phase abundances are larger for Model 2, mainly because s-CO desorbs from the grains in Model 2 in the molecular layer producing the other C-bearing species, while it stays on the grains in Model 1.

s-CH_3OH and s-H_2CO are efficiently formed at low T_{mid}: between 10 and 20 K, their abundances are respectively, ~10^{-5} and ~10^{-6}. Their main formation paths are:

$$\text{s-OH} + \text{s-CH}_3 \rightarrow \text{s-CH}_3\text{OH}, \quad (10)$$

$$\text{s-H} + \text{s-CH}_2\text{OH} \rightarrow \text{s-CH}_3\text{OH}, \quad (11)$$

$$\text{s-H} + \text{s-HCO} \rightarrow \text{s-H}_2\text{CO}, \quad (12)$$

$$\text{s-O} + \text{s-CH}_2 \rightarrow \text{s-H}_2\text{CO}. \quad (13)$$

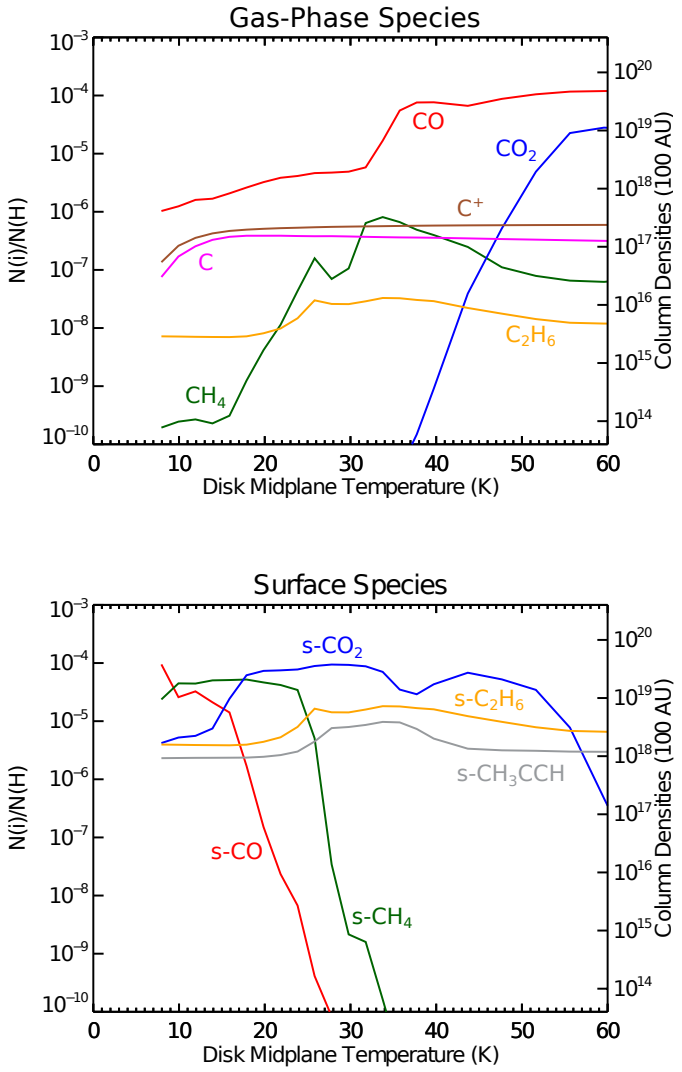

Fig. 4. Average abundances and integrated column densities (cm^{-2}) of carbon-bearing species in the gas phase and on the grain surfaces at 100 au as a function of the disk midplane temperature (T_{mid}). Results are for Model 1 and for a disk age of 1 Myr.

However, their abundances are strongly decreased at higher T_{mid} since s-H, s-HCO, s-O, and s-CH_2 are easily desorbed at such temperatures. The largest CH_3OH and H_2CO gas-phase column densities are found to be around 10^{12} cm^{-2} for T_{mid} = 20 K.

In summary, the carbon reservoir in protoplanetary disks strongly depends on the disk vertical temperature profile, which is controlled by the midplane temperature; the reservoirs are s-CO in the ices below 15 K, s-CO_2 in the ices between 15 and 30 K, and CO in the gas-phase above 30 K.

The results described above were obtained at 300 au. We now show the results of Model 1 (weak temperature gradient) at 100 au. In Fig. 4, are represented the disk abundances and column densities of carbon-bearing species in the gas-phase and on the grain surfaces at 100 au for Model 1 as a function of the disk midplane temperature (to be compared to Fig. 3). At 100 au, for a given vertical temperature profile, the density, the visual extinction, and the UV flux are larger than at 300 au. Considering the larger densities, the reservoirs of carbon at low temperature ($T_{mid} \leq 17$ K) are s-CH_4 and s-CO, and s-CO_2 between 17 and 34 K. At larger temperatures, gas-phase CO becomes dominant.

3.2. Photodesorption

Photodesorption was not included in our previous models. High desorption yields were found by Öberg et al. (2007), but it has been shown that the desorption efficiency depends on the shape of the UV spectrum (Fayolle et al. 2011). In particular, the photodesorption yield of CO ice induced by Ly-α photons is small (Chen et al. 2014).

We tested the impact of photodesorption on our results at 100 and 300 au for a disk age of 1 Myr. We used a large yield of 10^{-3} molecules photons^{-1} for all species except for CH_3OH, H_2O, CO_2, N_2, and CO for which we used the formalism described in Öberg et al. (2009a,b,c).

The carbon reservoir remains the same for both radii. The gas-phase CO abundance is only affected at 300 au for midplane temperatures between 4 and 15 K, with a CO abundance five times larger than in our nominal model. However, s-CO remains the main carbon-bearing species. For both radii, only more complex molecules, such as C_2H_6 and CH_3CCH, are efficiently photodesorbed (their abundances are increased by more than a factor 10).

3.3. Impact of the cosmic-ray ionization rate

Cosmic rays are important for the ionization in the disk. As recently suggested by Cleeves et al. (2013), however, cosmic ray penetration may be highly reduced in the presence of stellar winds and/or magnetic fields. In this section we study the impact of a lower (cosmic-ray) ionization rate on disk chemistry.

Figure 5 shows the abundances of the main carbon-bearing species for two values of the cosmic- ray ionization rate: 1.3×10^{-17} and 1.3×10^{-18} s^{-1} (in solid and dashed lines, respectively). The impact of the ionization rate on CO abundance is limited, as it is restricted to the temperature range 20–35 K. Considering the lower value for ζ_{CR}, s-CO abundance increases because its dissociation on the grain surface by UV photons induced by cosmic rays is less efficient. As a consequence, there is less carbon available to form s-CH_4. In the gas phase, the dissociation by secondary UV photons induced by cosmic ray/H_2 interactions is also less efficient so that CH_4 abundance increases at 300 au. At 100 au, the UV flux being larger, the direct photodissociation is the dominant process. CH_4 therefore presents similar sensitivity as s-CH_4 and decreases as well. We also ran our Model 1 for $\zeta_{CR} = 1.3 \times 10^{-19}$ s^{-1}, but the reservoirs remain the same as those shown in Fig. 5 (dashed lines) for both disk radii.

3.4. Impact of the age of the disk

The conversion of s-CO into more complex molecules on grains is a time-dependent process, which requires a minimum timescale to occur. Up to now, the results described were obtained for disks of 1 Myr. In this section we study the chemistry of carbon-bearing species for disks five times older.

Figure 6 shows the abundances of CO, s-CO, s-CO_2, and s-CH_4 obtained for Model 1 and for T_{mid} = 20 K, as a function of time. The s-CO abundance strongly decreases at 10^5 yr because of its conversion into other species, such as s-CO_2 and s-CH_4. We see that the formation of s-CH_4 requires a longer timescale to occur than the formation of s-CO_2. The species s-CH_4 reaches its highest abundance at 10^7 yr, while s-CO_2 is the most abundant species for a disk at an age of 10^6 yr. The reservoirs of carbon are therefore changed while considering an older disk.

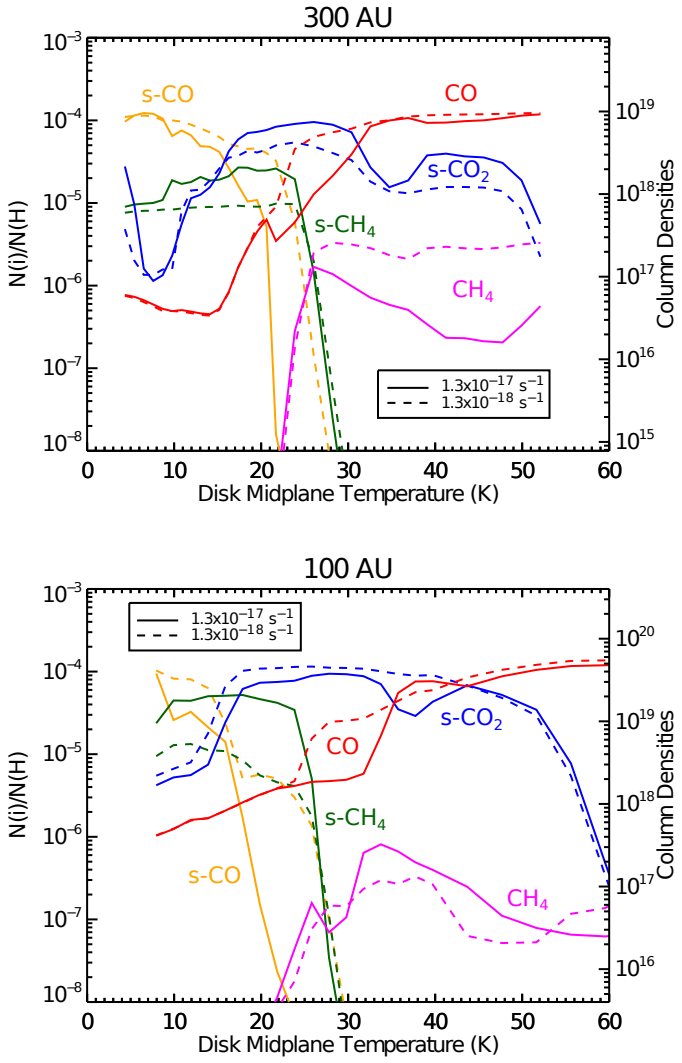

Fig. 5. Average abundances and integrated column densities (cm^{-2}) of main reservoirs of carbon at 300 au and 100 au for two values of the cosmic-ray ionization rate as a function of the disk midplane temperature (T_{mid}). Results are for Model 1 and for a disk age of 1 Myr.

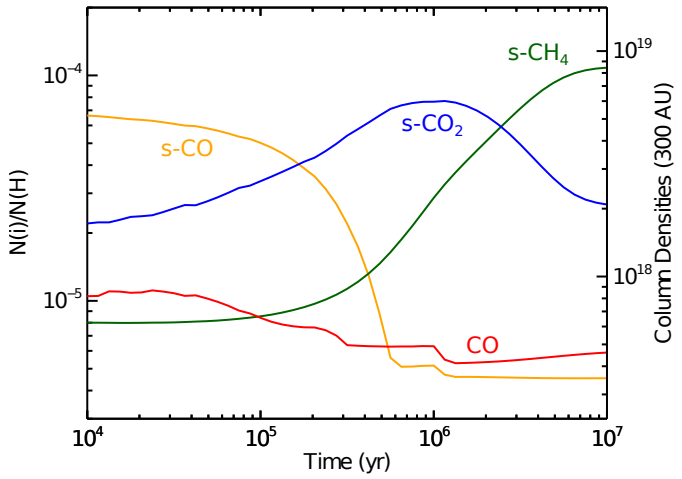

Fig. 6. Average abundances and integrated column densities (cm^{-2}) of main reservoirs of carbon at 300 au as a function of time. The results are obtained for Model 1 and for T_{mid} = 20 K at 300 au.

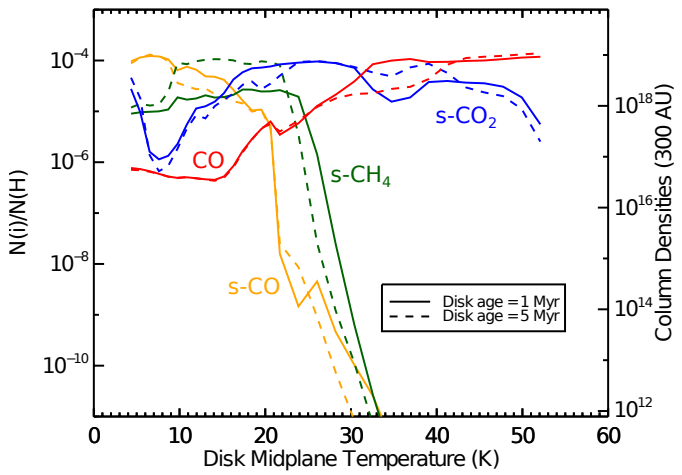

Fig. 7. Average abundances and integrated column densities (cm^{-2}) of main reservoirs of carbon at 300 au for two disk ages as a function of the disk midplane temperature (T_{mid}). Results are obtained for our Model 1.

Figure 7 represents the abundances and column densities of the main carbon-bearing species as a function of the disk midplane temperature for disks of 1 and 5 Myr. For the older disk, s-CH_4 is now the reservoir of carbon between 10 and 22 K in the midplane, which is due to its long formation timescale. The species s-CO_2 is also more abundant than CO between 32 and 40 K at 5 Myr compared to 1 Myr. This apparent dependency with temperature is actually a density effect. Because of the hydrostatic scale height, densities in the disk are smaller for higher temperatures, and the conversion time is just inversely proportional to the density. The conversion of CO into s-CO_2 is then longer in warmer disk so that at 35 K CO is the main carbon-bearing species for a disk of 1 Myr. For instance, in our model, this conversion timescale varies from 6×10^5 yr for disks at 25 K to 2×10^6 yr for disks at 35 K.

3.5. Sensitivity to the initial conditions

We now study the impact of the chemical composition of the parent molecular cloud on the disk chemistry. Several parameters have been studied such as gas density, C/O elemental ratio, and age of the parent cloud. The abundances of the main C-bearing species obtained for different cloud parameters, and used as initial conditions for the disk chemistry, are listed in Table 4. The results presented in this section are for disks of 1 Myr.

3.5.1. Density of the parent molecular cloud

To test the importance of the density of the parent molecular cloud, we redid our simulations but multiplied the density of the parent cloud by a factor of ten. The disk carbon chemistry is not very sensitive to the gas density of the parent molecular cloud. The reservoirs of carbon as described in the previous section are not changed. Only CH_3CCH abundance in the ices is decreased by a factor up to ~2 for all T_{mid} values.

3.5.2. C/O elemental ratio

For the carbon abundance, we use the value determined by Jenkins (2009) and we vary the C/O ratio by considering two different values for the oxygen elemental abundance: 1) 3.3×10^{-4} (value of our nominal model), a low depletion case; and 2) 1.4×10^{-4}, a high depletion case (see Sect. 2.1.2).

The reservoirs of carbon are not changed while using the high depletion case for C/O elemental ratio (C/O = 1.2). The only main difference is a smaller abundance of CO containing species and a larger abundance of CH containing species under some conditions. At 7 K, for instance, the CO, CH_4, and CO_2 abundances in the ices are 8.8×10^{-5}, 2.5×10^{-5}, and 3.8×10^{-7}, respectively.

3.5.3. Age of the parent molecular cloud

The age of molecular clouds is still a subject of debate. Ages are often considered between a few million years (Hartmann et al. 2001; Ballesteros-Paredes & Hartmann 2007) and 10 million years (Mouschovias et al. 2006). Ballesteros-Paredes & Hartmann (2007) suggested a short timescale of a few million years. They argued that as starless molecular clouds are rarely observed, star formation should occur shortly after cloud formation. Long cloud lifetimes have been favored because of the difficulty in explaining the sufficient formation of molecular hydrogen in only a few Myr, considering the slow rate at which H_2 forms in the ISM (Hollenbach et al. 1971). Glover & Mac Low (2007), however, suggested that turbulence significantly reduces the time required for the conversion of H into H_2 (less than 1–2 Myr). Pagani et al. (2011) suggested that the absence of DCO^+ in dark clouds is due to a high ortho-H_2 abundance, which provides an upper limit to the age of 3–6 million years. More recently, Brünken et al. (2014) used the abundance ratio of ortho-H_2D^+ and para-H_2D^+ and determined an age of dense molecular clouds around one million years.

To study the sensitivity of the model results to the age of the parent molecular cloud, we considered two additional cases. We computed the initial cloud composition at 10^5 yr and 10^7 yr, in addition to our standard model at 10^6 yr. In Fig. 8, we display the abundances and column densities of carbon-bearing species as a function of the disk midplane temperature computed with the different initial compositions. The abundances of the main C-bearing species obtained in the parent cloud at the different times (10^5, 10^6 and 10^7 yr) are listed in Table 4. The reservoirs of carbon in the disk are the same if a younger parent cloud is considered. However CO reaches its canonical value at larger $T_{\rm mid}$: 40 K instead of 32 K. In the case of an older cloud the reservoirs of carbon are changed. At temperatures smaller than 9 K for instance and in the case of a 10^7 yr cloud, CO in the ices is not the main C-bearing molecule anymore while CH_4 in the ices is the main C-bearing molecule. This can be explained by differences in the initial chemical composition of the cloud. The 10^5 and 10^6 yr compositions are similar and only the fraction between gas phase and surface CO is reversed. At the large density of the disks, the gas-phase CO is quickly depleted on the grains. At 10^7 yr in the cloud, the CO in the ices is hydrogenated to form H_2CO and CH_3OH in the ices, but is also photodissociated by secondary UV photons induced by cosmic rays and the atomic carbon is hydrogenated to s-CH_4. This means the reservoir of carbon in the disk remains CH_4 in the ices. At larger temperature, s-CO_2 is no longer the reservoir of carbon since CO_2 is formed on the surfaces from CO (already under abundant in the cloud) and the reservoir is C_2H_6 in the ices. To summarize, the reservoirs of carbon in a disk formed from an older molecular cloud with an age of 10^7 yr are CH_4 in the ices for temperature profiles computed with a $T_{\rm mid} < 22$ K and C_2H_6 in the ices for larger $T_{\rm mid}$.

The reservoir of carbon in disks is thus rather insensitive to initial conditions. The age of the cloud has an effect only if it is old enough, at least 10 Myr, a value on the high end of estimated cloud ages. In that case, s-CH_4 becomes the dominant C-bearing molecule instead of s-CO in the ices (for $T_{\rm mid} < 22$ K). For instance, for $T_{\rm mid} = 15$ K, the s-CH_4/s-CO ratio is ~5. This ratio is

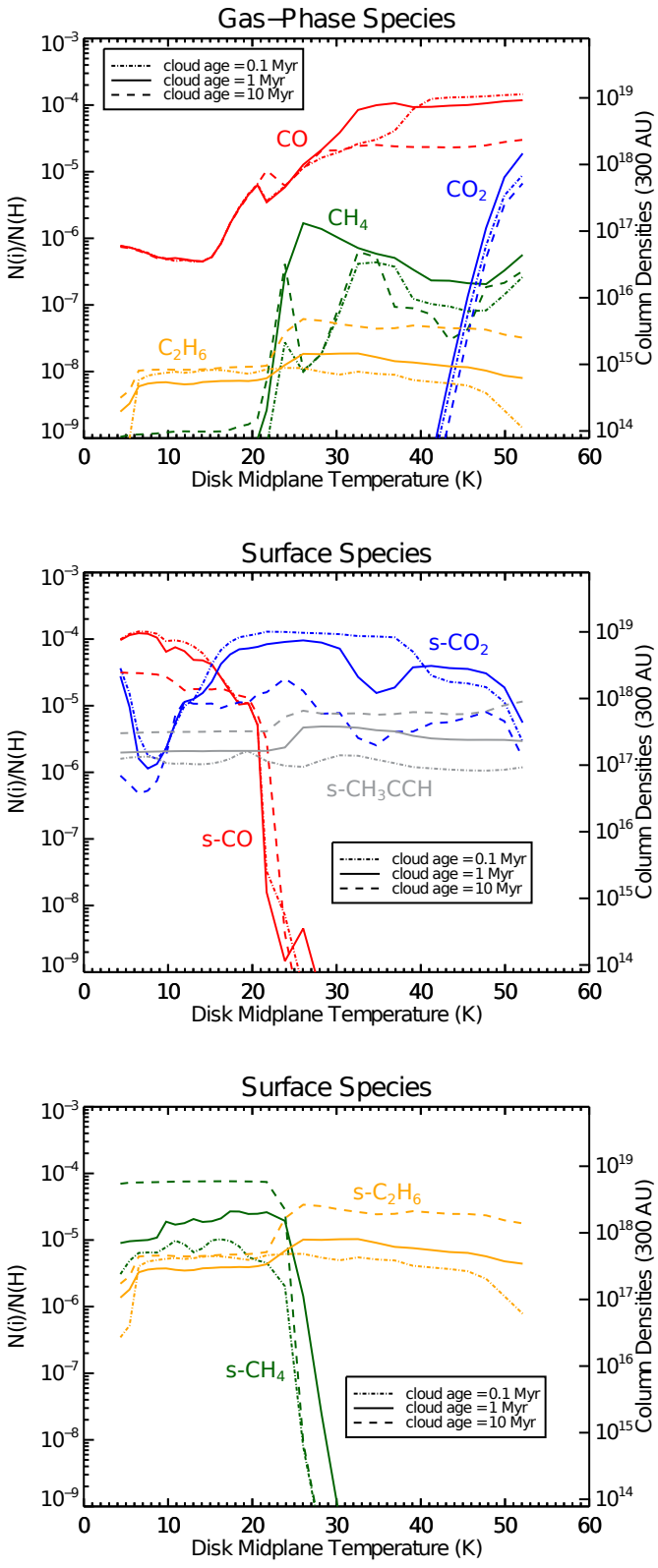

Fig. 8. Average abundances and integrated column densities (cm^{-2}) of carbon-bearing species in the gas-phase and on the grain surfaces for three ages of the parent molecular cloud as a function of the disk midplane temperature. Results are for Model 1 at 300 au, and for a disk age of 1 Myr. The results obtained for C and C^+ are not shown since the differences are very small.

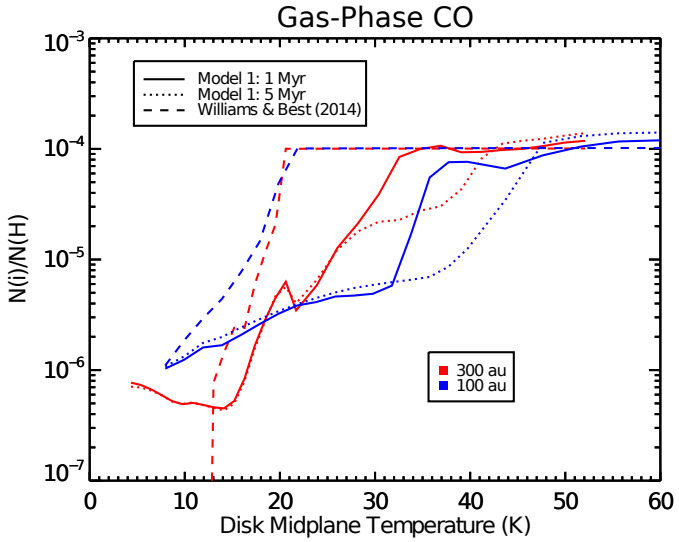

Fig. 9. Average abundance of gas-phase CO as a function of the disk midplane temperature ($T_{\rm mid}$). The results obtained with our Model 1 for disks of 1 and 5 Myr and at 100 and 300 au are compared to the model used by Williams & Best (2014) for CO chemistry.

much larger than those found in solar system comets (see Table 1 of Bockelée-Morvan et al. 2004), which may indicate that our solar system originates from a younger cloud.

4. Discussion

Transformation of CO into more complex species on grain surfaces was already invoked by Aikawa et al. (1997). In their study, however, the process is driven by neutral carbon and required enhanced X-ray ionization to be started. Ionized helium atoms react with CO to release C, which further reacts on grain surfaces to get s-CO_2 or other hydrocarbons. We have shown here that with a more complete grain chemistry, this mechanism is no longer necessary and CO can be converted to other forms even without enhanced ionization.

Our modeling reveals that, because of this processing on dust grains, the CO chemistry does not behave in a simple way. Figure 9 compares our average CO abundances with those predicted using the simple prediction of Williams & Best (2014), who assumed $CO/H_2 = 0$ where $T \leq 20$ K and in the photodissociation region, and $CO/H_2 = 10^{-4}$ elsewhere. Except for the coldest disks (where it predicts no CO), the simple prescription clearly overpredicts the average CO abundance for midplane temperatures below 30 to 35 K. At 20 K, the difference between our chemical model and the simple prescription is a factor of ~40. This suggests that gas-phase CO abundance is critically dependent on the (dust) temperature distribution and grain surface chemistry. Figure 9 shows that an abundance of 10^{-4} is only reached for disks with a midplane dust temperature above 30 K at 1 Myr and above 40 K at 5 Myr.

This complex CO chemistry may explain the low $C^{18}O$ to dust ratio observed in TW Hya by Favre et al. (2013). With an age estimate of 7–8 Myr (Barrado Y Navascués 2006; Ducourant et al. 2014)[2], TW Hya is old enough compared to the timescale required to convert CO to other forms on grain surfaces. To estimate the fraction of CO in gas phase quantitatively, a very accurate thermal model is needed. Hughes et al. (2008) reproduced the mm continuum and CO images of the TW Hya disk with two different disk models, a "cold" model with $T(r) = 30\ {\rm K}(r/100\ {\rm au})^{-0.5}$, and a "warm" solution with $T(r) = 40\ {\rm K}(r/100\ {\rm au})^{-0.2}$. We also note that Hughes et al. (2008) assume $T_{\rm dust} = T_{\rm gas}$, and the temperatures are certainly biased toward somewhat higher values because of the expected vertical temperature gradient and the difference between gas and dust temperatures. Nevertheless, for both cases, we would predict abundances of order 10^{-5}, in reasonable agreement with the results of Favre et al. (2013). Thus, there may be no need to invoke other mechanisms than the conversion of s-CO to s-CO_2 which is the dominant process in our study.

In comparison with other objects, CO depletion due to surface chemistry may not explain the apparent low CO-to-dust ratio derived by Chapillon et al. (2008) for the very warm disk of CQ Tau, where temperatures may exceed 50 K. However, Chapillon et al. (2008) only marginally resolved the source and their quoted temperatures are only for gas. Higher resolution studies, coupled with a more detailed thermal and chemical modeling for this source, would be needed to reach a conclusion.

We did not consider the very strong UV flux of Herbig Ae stars, so that a direct comparison between our results and any specific object is premature. Similarly, we only considered small grains. Larger grains reduce the gas-grain interactions, thereby augmenting the conversion timescale for CO, but as pointed out by Chapillon et al. (2008), these large grains could remain cooler. Also, turbulent mixing may play a role in bringing more frequently dust in the warm region, reducing the CO deficit. Turbulent mixing has been studied by Furuya & Aikawa (2014), and found to suppress the carbon depletion only within the inner 50 au. High CO content is thus expected in the inner regions (radius perhaps up to 30–50 au only). This is consistent with the CO/H_2 ratio about 10^{-4} derived from IR measurements by France et al. (2014) for RW Aur.

5. Conclusions

We have discussed the chemistry of carbon-bearing species in protoplanetary disks using our gas-grain chemical model Nautilus. In particular, we studied the effect of the disk temperature structure on the chemistry of carbon reservoir in disks. We also studied the impact of different initial parent cloud compositions. We found that the reservoir of carbon in disks is not sensitive to initial conditions such as gas density or C/O elemental ratio of the parent molecular cloud.

However, carbon chemistry is strongly sensitive to the disk vertical temperature profile. In many of our models, we have found that the CO gas-phase abundance is lower than the canonical value of $\sim 10^{-4}$ generally assumed. Indeed, with our models, these abundances are only reached for warm disks with a midplane temperature above 30 K, at 100 and 300 au for a disk age of 1 and 5 Myr. For smaller temperatures, we found that CO is converted into other species at the surface of the grains, such as s-CO_2, for which higher freeze-out temperatures prevent their desorption back into the gas-phase. The effect is slightly less efficient at a low cosmic-ray ionization rate (down to 1.3×10^{-18} s^{-1}) and large radii (300 au).

Finally, our work demonstrates that CO is not a simple tracer of H_2 in protoplanetary disks, because its abundance is very sensitive to the large (dust) temperature gradients that exist there. These gradients will be very difficult to constrain with sufficient

[2] A younger age of 3 Myr has been quoted by Vacca & Sandell (2011), but seems inconsistent with the dynamical age derived by Ducourant et al. (2014).

accuracy. Given the additional complexity of isotopologue selective photodissociation and fractionation, evaluating disk masses from measurements of the CO isotopologue emission alone will remain a very challenging task.

Acknowledgements. The authors thank the French CNRS/INSU program PCMI for their partial support of this work. V.W. and F.H. research is funded by the ERC Starting Grant (3DICE, grant agreement 336474). The authors also thank the referee for suggestions which helped to improve this paper.

References

Aikawa, Y., Umebayashi, T., Nakano, T., & Miyama, S. M. 1997, ApJ, 486, L51
Andrews, S. M., Rosenfeld, K. A., Kraus, A. L., & Wilner, D. J. 2013, ApJ, 771, 129
Ballesteros-Paredes, J., & Hartmann, L. 2007, Rev. Mex. Astron. Astrofis., 43, 123
Barrado Y Navascués, D. 2006, A&A, 459, 511
Bary, J. S., Weintraub, D. A., Shukla, S. J., Leisenring, J. M., & Kastner, J. H. 2008, ApJ, 678, 1088
Beckwith, S. V. W., Sargent, A. I., Chini, R. S., & Guesten, R. 1990, AJ, 99, 924
Bergin, E. A., Cleeves, L. I., Gorti, U., et al. 2013, Nature, 493, 644
Bockelée-Morvan, D., Crovisier, J., Mumma, M. J., & Weaver, H. A. 2004, in The composition of cometary volatiles, ed. G. W. Kronk (Tucson: University of Arizona Press), 391
Brünken, S., Sipilä, O., Chambers, E. T., et al. 2014, Nature, 516, 219
Chapillon, E., Guilloteau, S., Dutrey, A., & Piétu, V. 2008, A&A, 488, 565
Chapillon, E., Parise, B., Guilloteau, S., Dutrey, A., & Wakelam, V. 2010, A&A, 520, A61
Chen, Y.-J., Chuang, K.-J., Muñoz Caro, G. M., et al. 2014, ApJ, 781, 15
Chiang, E. I., & Goldreich, P. 1997, ApJ, 490, 368
Cleeves, L. I., Adams, F. C., & Bergin, E. A. 2013, ApJ, 772, 5
Ducourant, C., Teixeira, R., Galli, P. A. B., et al. 2014, A&A, 563, A121
Dutrey, A., Guilloteau, S., Duvert, G., et al. 1996, A&A, 309, 493
Dutrey, A., Guilloteau, S., & Simon, M. 2003, A&A, 402, 1003
Favre, C., Cleeves, L. I., Bergin, E. A., Qi, C., & Blake, G. A. 2013, ApJ, 776, L38
Fayolle, E. C., Bertin, M., Romanzin, C., et al. 2011, ApJ, 739, L36
France, K., Herczeg, G. J., McJunkin, M., & Penton, S. V. 2014, ApJ, 794, 160
Furuya, K., & Aikawa, Y. 2014, ApJ, 790, 97
Garrod, R. T., & Herbst, E. 2006, A&A, 457, 927
Garrod, R. T., Wakelam, V., & Herbst, E. 2007, A&A, 467, 1103
Glover, S. C. O., & Mac Low, M.-M. 2007, ApJ, 659, 1317
Graedel, T. E., Langer, W. D., & Frerking, M. A. 1982, ApJS, 48, 321
Guilloteau, S., Dutrey, A., Piétu, V., & Boehler, Y. 2011, A&A, 529, A105
Hartmann, L., Ballesteros-Paredes, J., & Bergin, E. A. 2001, ApJ, 562, 852
Hersant, F., Wakelam, V., Dutrey, A., Guilloteau, S., & Herbst, E. 2009, A&A, 493, L49
Hincelin, U., Wakelam, V., Hersant, F., et al. 2011, A&A, 530, A61
Hollenbach, D. J., Werner, M. W., & Salpeter, E. E. 1971, ApJ, 163, 165
Hughes, A. M., Wilner, D. J., Qi, C., & Hogerheijde, M. R. 2008, ApJ, 678, 1119
Hughes, A. M., Andrews, S. M., Espaillat, C., et al. 2009, ApJ, 698, 131
Jenkins, E. B. 2009, ApJ, 700, 1299
Lee, H.-H., Herbst, E., Pineau des Forets, G., Roueff, E., & Le Bourlot, J. 1996, A&A, 311, 690
Loison, J.-C., Wakelam, V., & Hickson, K. M. 2014a, MNRAS, 443, 398
Loison, J.-C., Wakelam, V., Hickson, K. M., Bergeat, A., & Mereau, R. 2014b, MNRAS, 437, 930
Miotello, A., Bruderer, S., & van Dishoeck, E. F. 2014, A&A, 572, A96
Mouschovias, T. C., Tassis, K., & Kunz, M. W. 2006, ApJ, 646, 1043
Öberg, K. I., Fuchs, G. W., Awad, Z., et al. 2007, ApJ, 662, L23
Öberg, K. I., Garrod, R. T., van Dishoeck, E. F., & Linnartz, H. 2009a, A&A, 504, 891
Öberg, K. I., Linnartz, H., Visser, R., & van Dishoeck, E. F. 2009b, ApJ, 693, 1209
Öberg, K. I., van Dishoeck, E. F., & Linnartz, H. 2009c, A&A, 496, 281
Pagani, L., Roueff, E., & Lesaffre, P. 2011, ApJ, 739, L35
Pérez, L. M., Carpenter, J. M., Chandler, C. J., et al. 2012, ApJ, 760, L17
Piétu, V., Dutrey, A., Guilloteau, S., Chapillon, E., & Pety, J. 2006, A&A, 460, L43
Piétu, V., Dutrey, A., & Guilloteau, S. 2007, A&A, 467, 163
Reboussin, L., Wakelam, V., Guilloteau, S., & Hersant, F. 2014, MNRAS, 440, 3557
Semenov, D., Hersant, F., Wakelam, V., et al. 2010, A&A, 522, A42
Vacca, W. D., & Sandell, G. 2011, ApJ, 732, 8
Wagenblast, R., & Hartquist, T. W. 1989, MNRAS, 237, 1019
Wakelam, V., & Herbst, E. 2008, ApJ, 680, 371
Wakelam, V., Smith, I. W. M., Loison, J.-C., et al. 2013, unpublished [arXiv:1310.4350]
Williams, J. P., & Best, W. M. J. 2014, ApJ, 788, 59